Supplementary Information Text

Appendix S1. Methods for compound specific stable isotope analysis

Collagen samples have been analyzed for both CSSIA and bulk $\delta^{15}N$ which require 10 mg of purified collagen (100 mg of bone). Preliminary analyses were conducted to determine the highest rate of collagen return from bone sampled from different parts of the skull to minimize destruction. Samples were taken from the internal occipital shelf to maintain external integrity. Bone was decalcified using 0.2 M HCl for 24-72 hours depending on bone thickness, followed by centrifugation and nanopure water rinse. Removal of humic acids was conducted using 0.125 M NaOH for 20 hours. Samples were washed to a neutral pH, then solubilized in 0.01N HCl. Once solubilized samples were blown down under N_2 to prevent isotopic fractionation, and freeze dried. Freeze dried collagen was be analyzed for bulk isotopic composition of nitrogen by the UW IsoLab (isolab.ess.washington.edu) using a coupled elemental analyzer-isotope ratio mass spectrometer following the standard protocols of the laboratory. C:N ratios were calculated from this data, which is a measure of the quality for carbon and nitrogen analyses of bone collagen for isotopic analysis. Only three observations were outside of the acceptable rang of 2.7-3.6; indicating there was no substantial loss of glycine or addition of nitrogen due to microbial processing from mortality, decay, curation, and analysis.

$\delta^{15}N$ of eleven amino acids[1] were measured in the UW Facility for Compound-Specific Isotope Analysis of Environmental Samples. Samples were prepared following the procedures developed by Chikaraishi et al. (2007) and protocols by Rachel Jeffreys lab at University of Liverpool UK which are modifications of that published by Metges and Petzke (1996) and Popp et al. (2007). Briefly, proteins were hydrolyzed in 6N HCl and purified using a cation exchange column. 20 μL or norleucine was added as an internal standard. Amino acids were esterified

[1] Alanine, glycine, proline, aspartic acid, leucine, isoleucine, valine, threonine, serine, glutamic acid, phenylalanine

using isopropanol acetyl chloride, and derivatized via acylation with 4:1 toluene: pivaloyl chloride. Samples were brought up in ethyl acetate and analyzed using a coupled gas chromatography-combustion-isotope ratio mass spectrometer system (GC-C-irMA; Thermo Scientific Trace GC + GC IsoLink coupled to a Delta V irMS) in continuous flow mode monitoring masses (m/z) 28 and 29. A 30 m x 0.32 mm x 0.50 μm Agilent Technologies DB-35 capillary column with 35% Phenyl and 65% polysiloxane stationary phase and moderate polarity was used (Chikaraishi et al. 2010) with an inlet temperature of 260 C, column flow of 2 ml/min and oven ramp of 9 ˚C min^{-1}. For each run a 12 amino acid external standard with known isotopic composition was injected four times followed by sample injections. Samples were injected in triplicate, with the 12 amino acid standard mixture injected every two samples (or six injections). A two-hour column oxidation was performed after 6 samples (25 injections) followed by a 30 minute backflush and conditioning using 4 standard injections.

For each machine run, a linear model was fit for each individual amino acid using the following equation:

$$Std_{aa} = m_{aa}t + b_{aa}$$

Where m represents the slope of the precision drift, t represents the injection number since last column oxidation, and Std represents the $\delta^{15}N$ of an individual amino acid for a standard observation. The data was then corrected using the following equations:

$$D_{aa,t} = Std_{aa,t} - True$$

Where $D_{aa,t}$ is the difference between an observed standard $\delta^{15}N$ ($Std_{aa,t}$) for a given amino acid at a given injection number and the true $\delta^{15}N$ for that standard. Then:

$$Sample_{corrected,aa,t} = Sample_{obs,aa,t} - D_{aa,t}$$

Where the drift value, $D_{aa,t,}$ is subtracted from the sample value for a given amino acid and a given injection to correct the observed sample values for precision drift since last column oxidation. Mean sample corrected values for the triplicate injections were used for all amino acid $\delta^{15}N$. Norleucine had lower precision in standards (mean = 0.4) compared to phenyalanine, therefore no correction using the internal standard was applied. Mean precision for a given AA standard was calculated using the standard deviation of the external standard injections for a given run after drift correction and taking a mean of each run's standard deviation. Conditioning injections were omitted from this calculation. Tyrosine and methionine (source amino acids) do not have a high enough concentration in bone collagen (Ho 1965) relative to other amino acids to be discernable by these methods. Additionally, lysine and histidine are not compatible with these methods. Data for serine and glycine were available but there is evidence that these amino acids exhibit trophic enrichment (Germain et al. 2013) and so we chose to omit them from this analysis and the accompanying dataset.

Appendix S2. Tissue turnover time assumption validation

To validate this approach of applying a 1-year lag, 2- and 3-year lags were also applied to the best models of each region an compared to the 1-year lag using AIC_c. A one-year tissue turnover time was confirmed as a suitable assumption for harbor seal bone collagen, as 2- and 3-year lags had similar or less model support for both and bulk $\delta^{13}C$ (Table S5) and $\delta^{15}N_{Phe}$ (Tables S6). Additionally, month was tested as a smoothed predictor with 12 knots for stable isotope data in Washington samples using a generalized additive model (GAM). Support for a significant smoothing term would identify and seasonality in the data, which would be expected if tissue turnover time is less than a year. There was no support for a smoothing effect by month in generalized additive models of $\delta^{15}N_{Phe}$ and $\delta^{13}C$ values which would have indicated any seasonal variability in isotope composition and thus a turnover time of less than or greater than a year ($p < 0.05$; SI Figure S2). Thus, a 1-year lag was applied to isotope data for all temporal analyses.

Appendix S3. Methods for Bayesian dynamic factor analysis using a Gaussian process model

Gaussian Processes (GP) have been widely used in fisheries and other fields (Munch et al. 2018). Instead of modeling a time series as an autoregressive process, GPs model a time series via a mean and variance function, $\boldsymbol{x} \sim MVN(\boldsymbol{u}, \boldsymbol{\Sigma})$ where $\boldsymbol{u}$ represents and optional mean vector and $\boldsymbol{\Sigma}$ a covariance matrix. For GPDFA, we assume the mean to be zero, letting just the covariance function determine the GP smoothing. GPs are flexible in that the covariance matrix can be described by a wide range of flexible functions; for this application we use a Gaussian kernel (squared exponential) so that $\Sigma_{i,j} = \sigma^2 \exp\left(-d_{i,j}/\theta\right)$, where σ^2 is a variance parameter controlling the magnitude, θ is a shape parameter controlling how quickly covariance declines, and $d_{i,j}$ is the known distance between time points *i* and *j*. A benefit of modeling $\boldsymbol{\Sigma}$ with a covariance function is that regardless of the dimensionality, all elements of $\boldsymbol{\Sigma}$ can be described by a small number of parameters. For GPDFA, we choose to use a GP predictive process model, because the number of time points may be large (e.g. Latimer et al. 2009). This predictive model estimates the function values at a subset of locations (knots), and combines these estimates with the distance to locations at which data are observed to make predictions. More specifically, the values of the time series at the knot locations are $\boldsymbol{x}^* \sim MVN(\boldsymbol{0}, \boldsymbol{\Sigma}^*)$. Given the known distances between the locations of knots and locations of data, the covariance matrix between the two can be calculated, $\Sigma_{(x,x^*)}$. Finally, the predictions of the time series at the observed data can be calculated as $\hat{x} = \Sigma'_{(x,x^*)} \Sigma^{*-1} x^*$. In this extension of DFA, all other model components are identical to the conventional time series version with latent trends modeled as a random walk.

With the Gaussian Process DFA model, a decision needs to be made a priori about selecting the number and location of knots, where the function parameters are estimated at. There are multiple approaches for doing this; we adopted a model with 15 knots (more knots resulting

in a smoother function), and estimated the knot location by performing a clustering approach of the years corresponding to the raw observations (partitioning around medoids, using the 'pamk' function in the fpc library in R).

Table S1: Environmental datasets. SST data was obtained from NOAA_ERSST_V5 data provided by the NOAA/OAR/ESRL PSD, Boulder, Colorado, USA, from their Web site at *https://www.esrl.noaa.gov/psd/* (Huang et al. 2017).

Environmental Driver Category	Eastern Bering Sea	Gulf of Alaska	Washington
Discharge	Total discharge from the Kuskokwim River at Crooked Creek, AK during the winter months of low discharge (Nov-Apr) and summer months of high discharge (May-Oct) from monthly U.S. Geological Survey discharge data. 1951-2018. **N = 3** Data Source: USGS 15304000	Estimates of total freshwater discharge for a location near Seward, Alaska during winter months of low discharge (Jan-Jul) and summer months of high discharge (Aug-Dec) from monthly data. 1931-2011. **N= 3.** Data Source: Tom Royer, Royer and Grosch 2007	Total discharge from the Columbia River at Dalles, WA and Fraser River at Hope during the winter months of low discharge (Nov-Apr) and summer months of high discharge (May-Oct) from monthly U.S. Geological Survey discharge data. 1879-2018 and 1913-2016. **N= 6.** Data Source: USGS 14105700; BC Fraser 08MF005
Sea Surface Temperature (SST)	Average of monthly NOAA Extended Reconstructed SST for winter (Jan-Mar), spring (Apr-Jun), summer (Jul-Sep), and fall (Oct-Dec) and annually at 60°N, 170°W. 1854-2019. **N = 5** Data Source: NOAA ERSST V5	Average of monthly NOAA Extended Reconstructed SST for winter (Jan-Mar), spring (Apr-Jun), summer (Jul-Sep), and fall (Oct-Dec) and annually in southcentral AK (60°N 149°W). 1854-2019. **N = 5** Data Source: NOAA ERSST V5	Average of monthly NOAA Extended Reconstructed SST for winter (Jan-Mar), spring (Apr-Jun), summer (Jul-Sep), and fall (Oct-Dec) and annually in coastal Washington (48°N, 125°W). 1854-2019. **N=5** Data Source: NOAA ERSST V5
Upwelling/Circulation	Average winter (Oct-Apr) cross-shelf and along-shelf wind at 60°N, 170°W from monthly NCEP/NCAR reanalysis data. 1949-2011. **N = 2** Data Source: Megan Stachura, Stachura et al. 2014 from NOAA ESRL Mean annual sea ice extent in the Bering Sea from 1850-2017 from National Snow and Ice Center Data Source: NSIDC (Walsh et al. 2019)	Mean coastal upwelling index (CUI) the Gulf of AK (60°N, 149°W and 60°N, 147°W) using Bakun upwelling calculation based on Ekman's theory of mass transport due to wind stress, for spring and summer. 1946-2019. **N = 4** Data Source: NOAA ERD SWFSC	Mean coastal upwelling index (CUI) coastal Washington (45°N, 125°W) using Bakun upwelling calculation based on Ekman's theory of mass transport due to wind stress, for spring, summer, winter and annual. 1946-2019. Data Source: NOAA ERD SWFSC Total upwelling magnitude Index (TUMI, 45°N). 1965-2019. Data Source: NOAA CCIEA
Climate Regime	Multivariate ENSO Index (1950-2019), Oceanic Nino Index (1950-2019), Pacific Decadal Oscillation Index (1900-2018), the Northern Oscillation Index (1928-2019), North Pacific Gyre Oscillation (1950-2019). **N = 5** Data Sources: PDO; NPGO; NOI; MEI; ONI	Same as eastern Bering Sea	Same as eastern Bering Sea

Table S2: Time series subsets for linear models by regions.

Mechanism	Washington	Gulf of Alaska	Eastern Bering Sea
Climate Regime	Pacific Decadal Oscillation	Pacific Decadal Oscillation	Pacific Decadal Oscillation
Climate Regime	Multivariate ENSO Index	Multivariate ENSO Index	Multivariate ENSO Index
Climate Regime	North Pacific Gyre Oscillation	North Pacific Gyre Oscillation	North Pacific Gyre Oscillation
Temperature	Mean summer sea surface temperature (Jul-Sep) at 48°N, 125°W	Mean summer sea surface temperature (Jul-Sep) at 60°N 149°W	Mean summer sea surface temperature (Jul-Sep) at 60°N, 170°W
Circulation	Mean summer coastal upwelling (Jul-Sep) at 48°N, 125°W	Mean summer coastal upwelling (Jul-Sep) at 60°N 149°W	Mean winter (Oct-Apr) cross-shelf wind vector at 60°N, 170°W
Circulation	Mean Coastal Upwelling (Spring)	Mean Coastal Upwelling (Spring)	Average winter (Oct-Apr) along-shelf wind vector at 60°N, 170°W
Discharge	Columbia River Discharge during summer months of high discharge (May-Oct)	Total freshwater discharge for a location near Seward during summer months of high discharge (May-Oct)	Total discharge from the Kuskokwim River at Crooked Creek during summer months of high discharge (May-Oct)

Table S3: Pairwise t-test by sub region with bonferroni correction and pooled standard deviation for $\delta^{15}N_{Phe}$ values.

	Eastern Bering Sea	Coastal WA	Salish Sea	Northern GoA
Coastal WA	**p < 0.05***	-	-	-
Salish Sea	**p < 0.05***	**p < 0.05***	-	-
Northern GoA	**p < 0.05***	1.00	1.00	-
Southeast GoA	**p < 0.05***	1.00	**p < 0.05***	0.52

Table S4: Pairwise t-test by sub region with bonferroni correction and pooled standard deviation for $\delta^{13}C$ values.

	Eastern Bering Sea	Coastal WA	Salish Sea	Southcentral GoA
Coastal WA	1.00	-	-	-
Salish Sea	**p < 0.05***	**p < 0.05***	-	-
Northern GoA	**p < 0.05***	**p < 0.05***	**p < 0.05***	-
Southeast GoA	**p < 0.05***	**p < 0.05***	**p < 0.05***	1.00

Table S5: Covariates and AIC_c values for models with the most support for $\delta^{13}C$ applying 1, 2, and 3 year lags. **Bold** indicates models with the most support for a subregion ($delAIC_c > 2$) and *italics* indicates models with similar support ($delAIC_c < 2$; more than one lag has similar support) for a subregion.

	Lag 1	Lag 2	Lag 3
Washington	*Discharge, Upwelling, PDO (276.75)*	PDO, MEI, Upwelling (284.62)	***PDO, Upwelling (276.12)***
Gulf of Alaska	***PDO, NPGO (188.57)***	*Upwelling, NPGO (189.81)*	Upwelling, PDO, NPGO (201.37)
Eastern Bering Sea	**U (38.1)**	U, NPGO (41.4)	U, NPGO (41.44)

Table S6: Covariates and AIC_c values for models with the most support for $\delta^{15}N_{Phe}$ applying 1, 2, and 3 year lags. **Bold** indicates models with the most support for a subregion and *italics* indicates models with similar support ($delAIC_c < 2$; more than one lag has similar support) for a subregion.

	Lag 1	Lag 2	Lag 3
Washington	*Discharge, Upwelling (367.81)*	***SST, PDO, NPGO (366.88)***	*SST, PDO, Upwelling (366.92)*
GoA	***Upwelling, Location (361.31)***	*Location (361.52)*	*Location (361.52)*
EBS	**Null (61.1)**	Null (67.90)	Null (73.46)

Figure S1: Analysis of a) $\delta^{15}N_{Source}$ and b) $\delta^{13}C$ values by month. For both models, s(month) $p > 0.1$ indicating no seasonality of harbor seal bone collagen stable isotope signature.

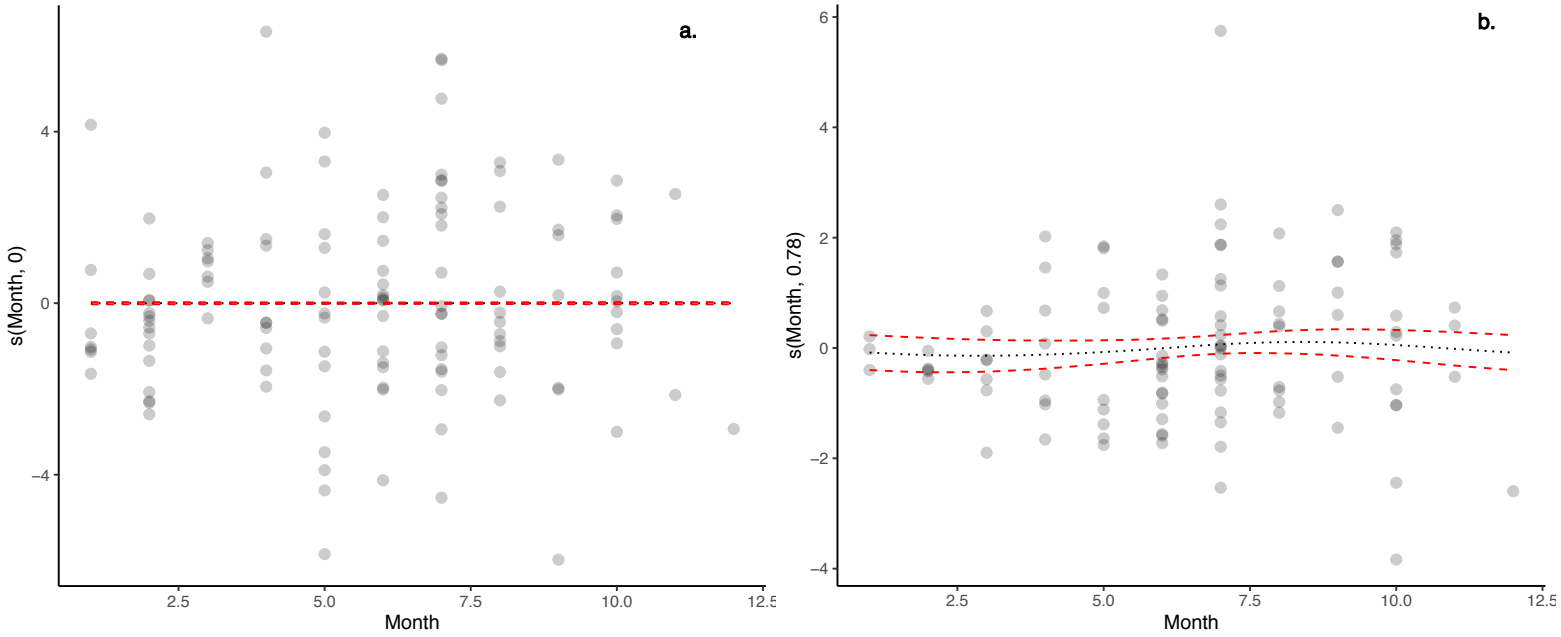

Figure S2: Analysis of a) $\delta^{15}N_{Source}$ and b) $\delta^{13}C$ values by length. For both models, there was no significant slope ($p>0.1$)

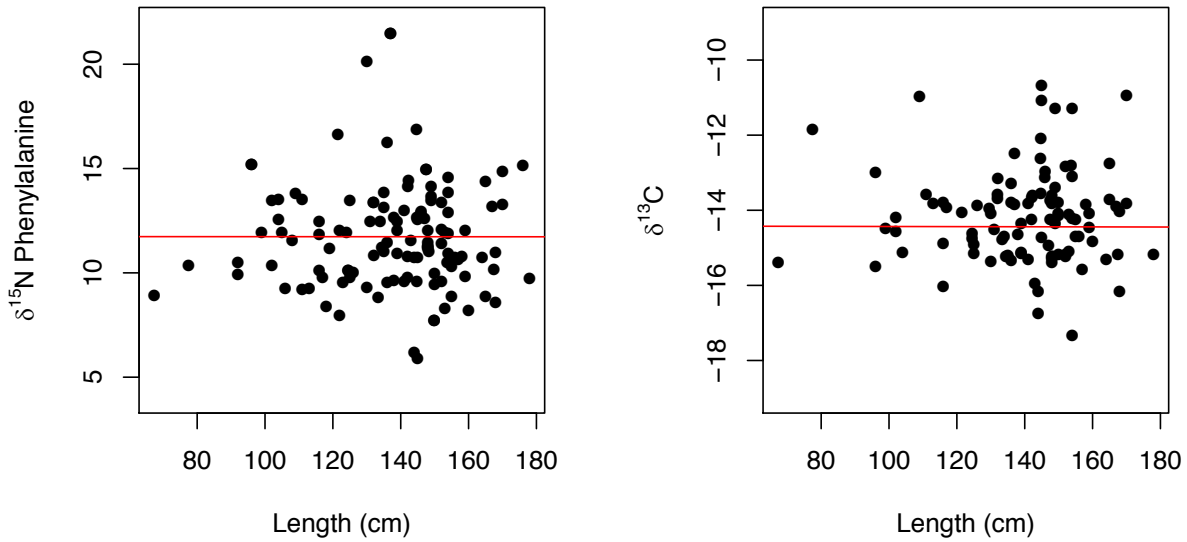

Figure S3: Bone collagen $\delta^{15}N$ values of phenylalanine from archival harbor seal specimens collected in the northeastern Pacific in five subregions.

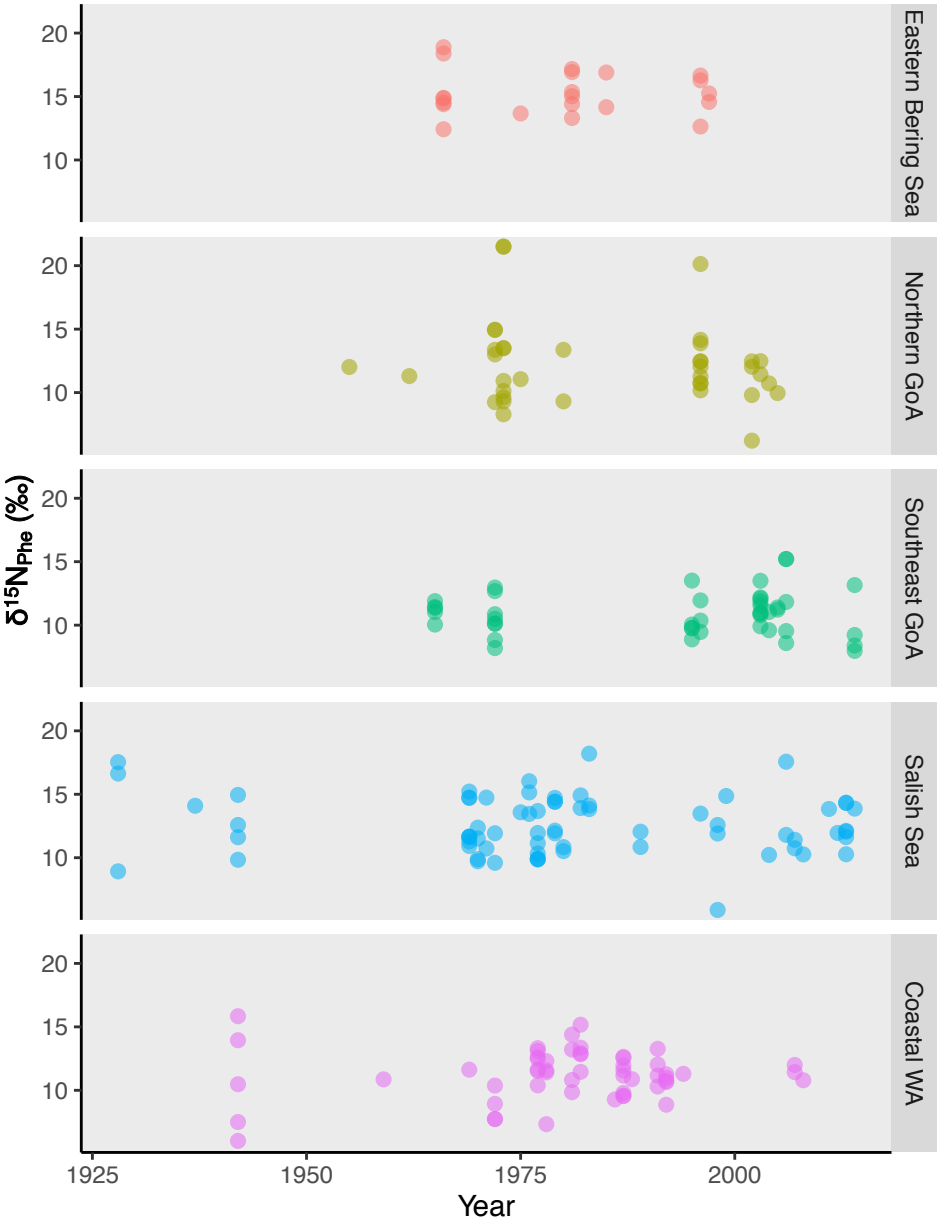

Figure S4: Bone collagen bulk $\delta^{13}C$ values of archival harbor seal specimens collected in the northeastern Pacific in five subregions. These values are not corrected for the Suess effect.

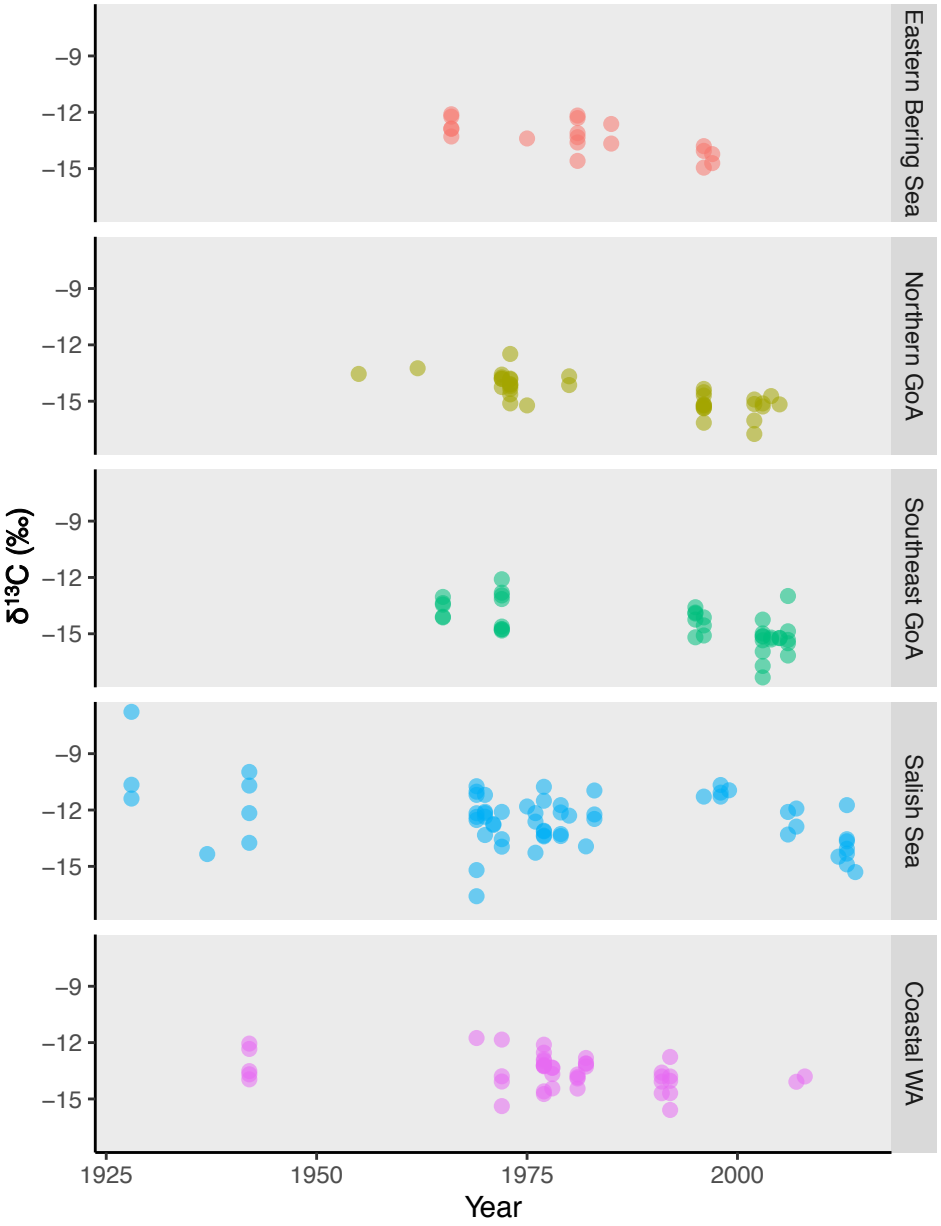

Figure S5: Bone collagen bulk $\delta^{13}C$ values of archival harbor seal specimens collected in the northeastern Pacific in five subregions. These values are corrected for the Seuss effect.

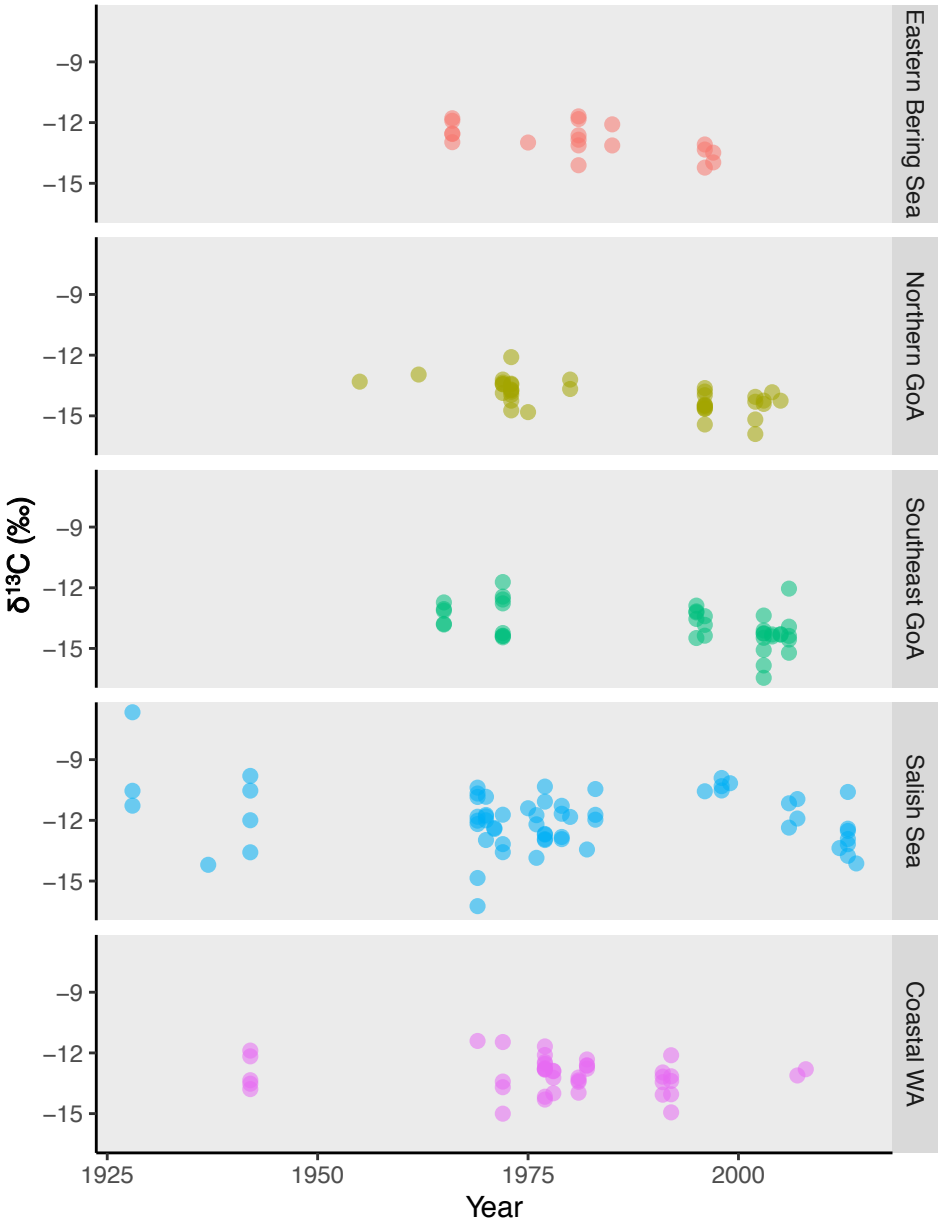

Figure S6: Bone collagen bulk $\delta^{15}N$ values of archival harbor seal specimens collected in the northeastern Pacific in five subregions.

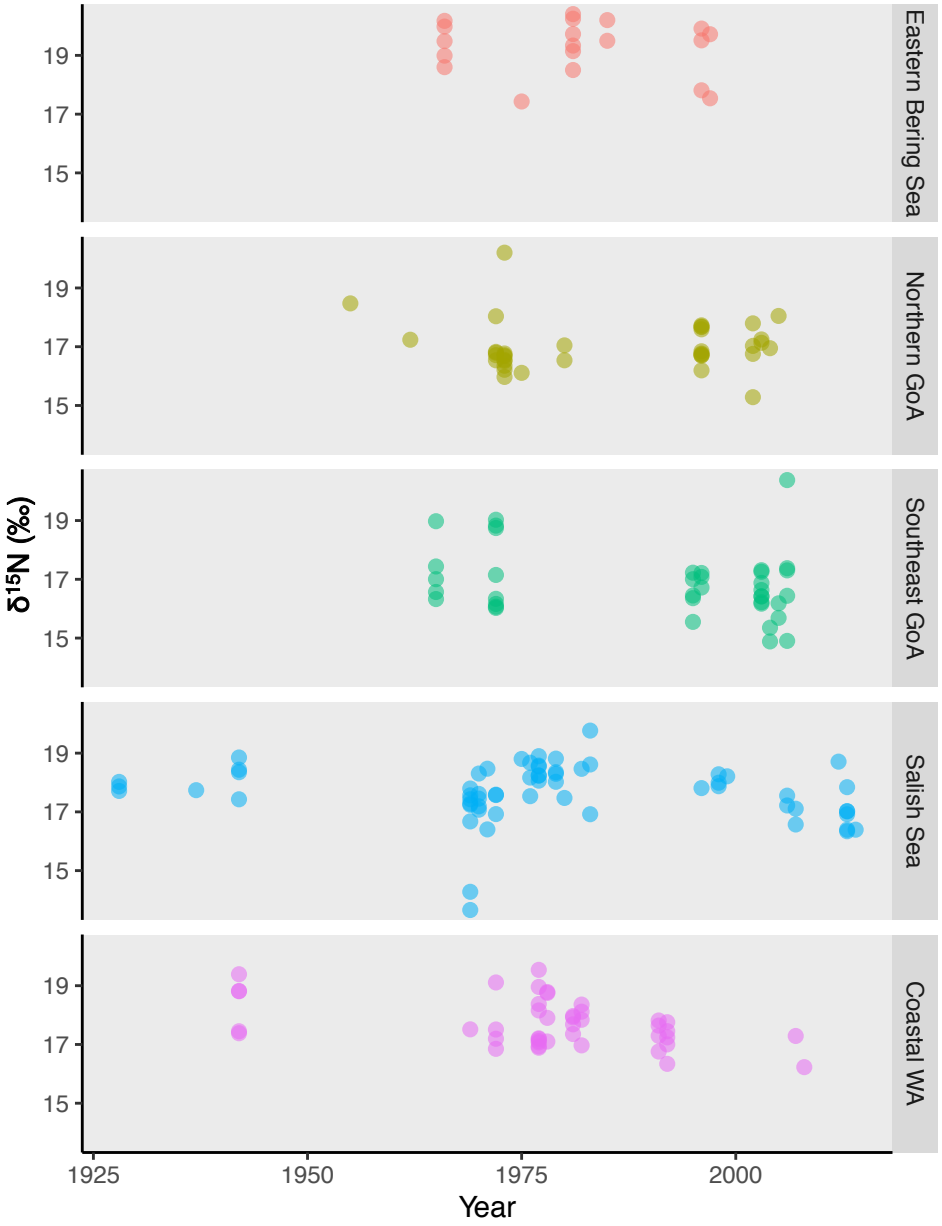

Figure S7: Residuals for the model with the most support (Figure 5) plotted by year. A trend in model residuals would indicate environmental variables do not account for all temporal variation in harbor seal $\delta^{15}N_{Phe}$ and $\delta^{13}C$ values.

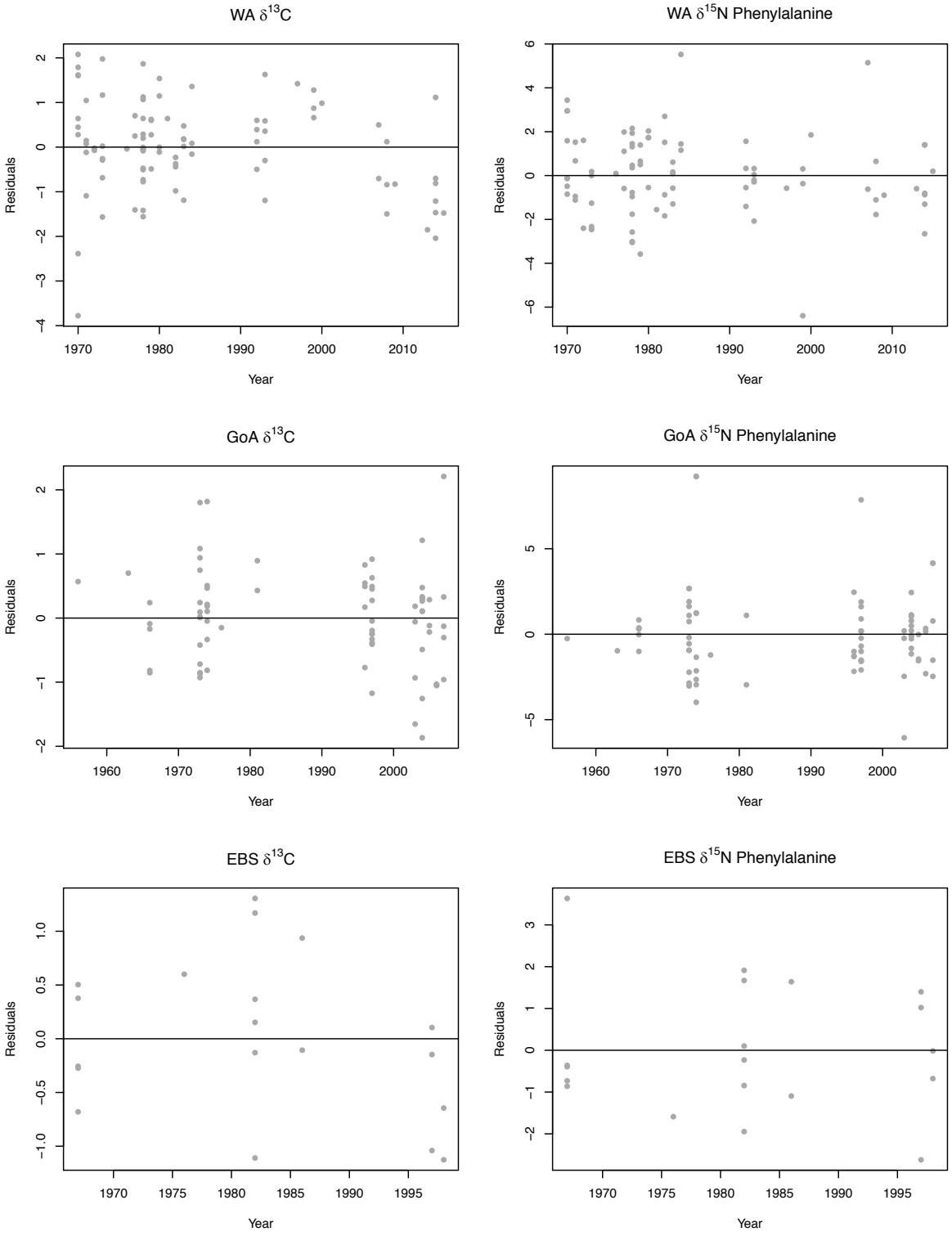

Figure S8: Model residual plots for the models with the most support from the candidate model set described in Table S3. Note: EBS phenylalanine is an intercept only model, GOA phenylalanine only contains a 2-factor location as a covariate.

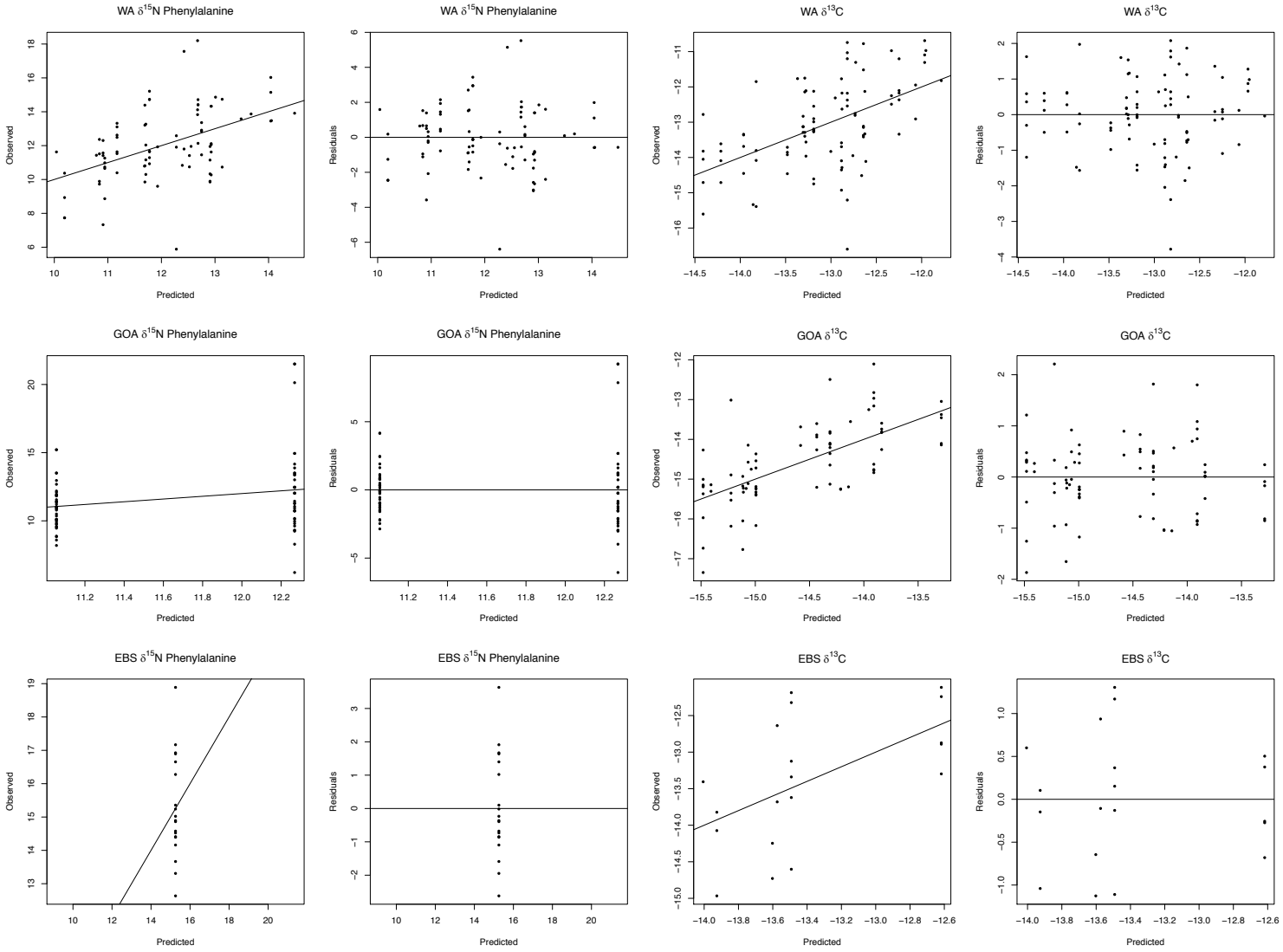

References

Chikaraishi Y., Kashiyama, Ogawa N.O., Kitazato H., Ohkoushi N. (2007). Metabolic control of nitrogen isotope composition of amino acids in macroalgae and gastropods: implications for aquatic food web studies. *Marine Ecology Progress Series* **342**, 85-90.

Chikaraishi Y., Takano Y., Ogawa N.O., Ohkouchi N. (2010). Instrumental optimization of compound-specific nitrogen isotope analysis of amino acids by gas chromatography/combustion/isotope ratio mass spectrometry. In: Tayasu I., Ohkouchi N. Keisuke K. (Eds.) Earth, Life, and Isotopes (pp. 367- 386). Kyoto University Press.

Germain L.R., Koch P.L., Harvey J., McCarthy M.D. (2013). Nitrogen isotope fractionation in amino acids from harbor seals: implicatios for compound-specific trophic position calculations. *Marine Ecology Progress Series* **482**, 265-277.

Huang B., Thorne P.W., Banzon V.F., Boyer T., Chepurin G., Lawrimore J.H., Menne M.J., Smith T.M., Vose R.S., Zhang H. (2017). NOAA Extended Reconstructed Sea Surface Temperature (ERSST), Version 5. NOAA National Centers for Environmental Information. doi:10.7289/V5T72FNM

Latimer A.M., Banerjee S., Sang Jr H., Mosher E.S., Silander Jr J.A. (2009). Hierarchical models facilitate spatial analysis of large datasets: a case study on invasive plant species in the northeastern United States. *Ecology Letters* **12**, 144-154.

Metges C.C., Petzke K. (1996). Gas chromatography/combustion/isotope ratio mass spectromic comparison of *N*-Acetyl- and *N*-Pivaloyl amino acid esters to measure ^{15}N isotopic abundances in physiological samples: a pilot study on amino acid synthesis in the upper gastro-intestinal tract of minipigs. *Journal of Mass Spectrometry* 31, 367-376.

Munch S.B., Giron-Nava A., Sugihara G. (2018). Nonlinear dynamics and noise in fisheries recruitment: A global meta-analysis. *Fish and Fisheries* **19**, 964-973.

Popp B.N., Graham B.S., Olson R.J., Hannides C.C.S., Lott M.J., López-Ibarra G.A., Galván-Magaña F., Fry B. (2007). Insights into the trophic ecology of yellowfin tuna, *Thunnes albacores*, from compound-specific nitrogen isotope analysis of proteinaceous amino acids. *Terrestrial Ecology* 1, 173-190.

Stachura M.M., Essington T.E., Mantua N.J., Hollowed A.B., Haltuch M.A., Spencer P.D., Branch T.A., Doyle M.J. (2014). Linking Northeast Pacific recruitment synchrony to environmental variability. *Fisheries Oceanogrpahy* **23**, 389-408.

Walsh J. E., Chapman W.L., Fetterer F., Stewart J.S. (2019). Gridded Monthly Sea Ice Extent and Concentration, 1850 Onward, Version 2. Boulder, Colorado USA. NSIDC: National Snow and Ice Data Center.